(*e*,2*e*) ionization studies of the stable noble gases in a coplanar symmetric geometry

Kate L. Nixon* and Andrew James Murray†

Photon Science Institute, School of Physics and Astronomy, University of Manchester, Manchester M13 9PL, United Kingdom

(Received 24 January 2013; published 26 February 2013)

A comprehensive set of coplanar symmetric (*e*,2*e*) ionization data are presented for the stable noble gas targets helium, neon, argon, krypton, and xenon. The incident electron energy ranged from 1.2 to 200 eV above the ionization potential of the target atoms, so as to span from near threshold to the high-energy regime. Data are presented with high precision, and cover a wide angular range from forward scattering where the electrons were detected at angles from 30° to the incident electron beam, through to the backscatter region where the deflection angle was up to 130°. The data are normalized to unity at each energy, and are compared to previously published theoretical calculations where available. The data show complex changes in the structure of the measured cross sections, depending upon both the energy and selected target. Similarities and differences in the cross sections were found between the different targets, which provide a challenge to future models of the ionization process.

DOI: 10.1103/PhysRevA.87.022712 PACS number(s): 34.80.Dp

I. INTRODUCTION

In a recent publication [1] a detailed set of experimental data was presented for electron impact ionization of the stable noble gases from near threshold to intermediate energies, where the scattered and ejected electrons emerged in the perpendicular plane ($\psi = 90°$; see Fig. 1). A number of unusual features were found, which could not be described by the simple binary and recoil scattering mechanisms used to explain ionization of helium in this regime. In particular, the heaviest target (xenon) displayed anomalous behavior that did not follow the general trends observed for lighter targets.

Further studies were carried out from xenon, with the incident electron momentum varying from $\psi = 0°$ (coplanar geometry) through to $\psi = 90°$ [2]. Additional structures in the differential cross section (DCS) were again found, in particular in the region where the electrons emerge in opposite directions to each other within the detection plane ($\xi \sim 90°$). These results were compared to the calculation by Purohit *et al*. using a distorted wave Born approximation (DWBA) [3], and there was little agreement between theory and experiment. Purohit and co-workers carried out further DWBA calculations from neon and argon in the perpendicular plane [4], and included postcollisional interactions (PCI) and target polarization in their model. Inclusion of polarization had only a small effect on the calculation for neon (static polarization $2.68a_0^3$); however, it significantly altered the predicted cross section for argon (static polarization $11.1a_0^3$ [5]) at low energy. In particular, inclusion of polarization produced the observed central maximum at a mutual angle $\phi = 2\xi = 180°$; however, it also resulted in a dramatic *decrease* in the cross section at other angles, contrary to the experimental data. In general, the calculation was in better agreement with experiment at higher energies. However, none of the calculated cross sections predict the data over all energies.

Illarionov and Stauffer [6] recently used a fully relativistic theory within a Dirac-Fock framework to calculate the ionization cross sections from xenon. Their relativistic approach should improve the accuracy of the calculation, due to the heavy nature of this target. At the highest energies some agreement was found between theory and experiment; however, in most cases the calculation once again did not accurately reproduce the data. This was particularly noticeable at the lowest energies where theory predicts a *maximum* cross section when the data shows a minimum. The relativistic calculation did not include target polarization (which is large in xenon with a static polarization $27a_0^3$), nor did it include second-order terms in the Born approximation. Both of these may play a significant role for this target.

The poor agreement between the predictions of these sophisticated models and the data prompted the further experimental studies that are presented here. To simplify the scattering dynamics a coplanar geometry has been chosen, where the incident, scattered, and ejected electron momenta all lie in the detection plane ($\psi = 0°$). Since there is then no resulting electron momentum out of the plane, the scattering processes that lead to ionization should be less complex than for studies in the perpendicular plane. In the work presented here, the incident electron energy $E_{\rm inc}$ ranged from 1.2 eV above the ionization potential (V_I) to 200 eV above V_I. A coplanar symmetric geometry was chosen ($\xi_1 = \xi_2 = \xi$) with the outgoing electrons carrying equal energy from the reaction ($E_1 = E_2 = E$, $E_{\rm inc} = 2E + V_I$). This geometry was chosen as it has a common point of normalization with the perpendicular plane when $\xi = 90°$. A direct comparison of the relative magnitude of the cross sections in both coplanar and perpendicular geometries can then be made.

This paper is divided into four sections. Following this introduction a brief description of the experimental procedure used to collect those data is given. Data for ionization of helium in a coplanar symmetric geometry are then presented for comparison to the heavier targets. Results from neon, argon, krypton, and xenon are then given, after which conclusions are drawn about the results that have been obtained. Where possible, the data are compared to published theoretical calculations at or near the energies that have been used in the present study.

*Email address: Kate.Nixon-2@manchester.ac.uk
†Email address: Andrew.Murray@manchester.ac.uk

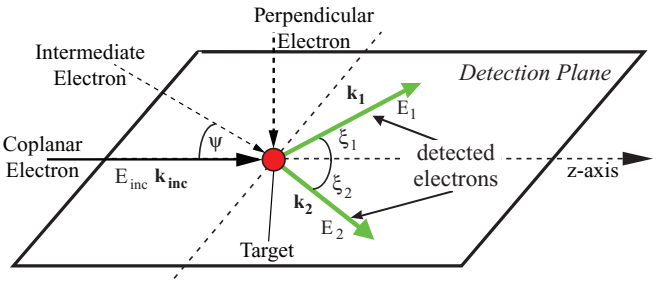

FIG. 1. (Color online) The experimental geometry adopted in this study. The electron gun and analyzers all lie in the detection plane, so that $\psi = 0^\circ$. The incident electron of energy $E_{\rm inc}$ defines the z axis. The outgoing electrons are detected at equal angles $\xi_1 = \xi_2 = \xi$ with respect to this axis, and are selected to have equal energy so that $E_1 = E_2 = E$. Since ionization is from the ground state of the target to the ground state of the ion with an ionization potential V_I, the energies are related through $E_{\rm inc} = V_I + 2E$.

II. EXPERIMENTAL PROCEDURES

The spectrometer used for these studies has been extensively described in the literature [7,8] and so will not be detailed here. The experiments were all carried out with an operating vacuum pressure of $\sim 1 \times 10^{-5}$ Torr, using a range of electron beam currents from <100 nA to more than 4 μA. The beam current was varied so as to optimize the signal-to-noise ratio when collecting coincidence data, so only relative measurements of the cross section were obtained. All data presented here are hence normalized to unity at the peak of the cross section at any given energy.

The incident electron energy was initially calibrated using the 19.334 eV elastic scattering resonance in helium. The pass energy of the scattered and ejected electron energy analyzers was then set by measuring the position of inelastic scattering peaks, and by carrying out binding energy scans of the coincidence spectra to confirm the ionization potential [9]. These energy calibrations were regularly carried out during data collection over a period of $\sim$6 months. Once the residual energies of the electron analyzers were determined for helium, these were used to set the energy of the experiments during data collection from different targets. This was necessary as the introduction of different gases into the spectrometer could change the effective energy of the electron beam, due to ionization and scattering effects near the emitting cathode, and due to adsorption of gas onto surfaces. This latter effect could change the relative potential of a surface, particularly in regions where the electron beam density was high and the electron energy was low. Since the electron density is negligible inside the analyzers, the analyzer residual energies did not suffer from the introduction of different gases, and so were used as an overall energy reference.

The energy range adopted for each target also varied, due to the difficulty of working with electron beams in this regime, and due to the challenges associated with detecting electrons of low energy. The measured cross sections varied by up to three orders of magnitude, and the coincidence count rates ranged from a few counts per second down to less than one count in several hundred seconds, again depending upon the target and incident energy adopted. Such low count rates prove challenging, as the signal-to-noise ratio is correspondingly small. Under long operating times the spectrometer stability is important, and so the data presented here are the accumulation of many sweeps of the detection plane. To ensure good statistical accuracy, data was hence accumulated over a complete sweep of the detection plane for different times at each angle, depending upon the detected rate. Over a single sweep, variations in pressure and current were insignificant, and so the data were renormalized to a common collection time. For the full set of data over many sweeps of the detection plane, the long-term variation in current and vacuum pressure could change by $\sim$5%. For small current changes, the count rate is proportional to the incident current, and so data accumulated over a given sweep were renormalized to the average beam current for that sweep. The changes in pressure produced changes in the count rate that were smaller than normal statistical variations, and so were ignored. The uncertainties in the final data presented in Figs. 2–6 were then derived from the variation in the overall mean for each angle.

III. (e,2e) DATA IN A COPLANAR SYMMETRIC GEOMETRY

Data for the ionization of helium in a coplanar symmetric geometry are initially presented so a comparison can be made to results from other targets. Helium has a 1^1S_0 ground state with both electrons occupying orbitals with $l = 0$. Single ionization of helium hence leaves an ion in the $1^2S_{1/2}$ state, with the bound electron in the He^+ ion having $l = 0$.

By contrast, all other noble gases have outer electrons occupying p orbitals. In each case the total angular momentum of the target ground state is $L = 0$ so that the atoms are again in an n^1S_0 state, with $n = 2$ (neon), $n = 3$ (argon), $n = 4$ (krypton), and $n = 5$ (xenon). Single ionization of a valence electron then leaves the ion in an n^2P_J state, with $J = 1/2$ or $J = 3/2$. In all cases apart from xenon, the spectrometer could not resolve the ionization yield to these individual ion states and so the presented data are in the form of a sum over both states. Since the ionized electron is a p electron for the heavier atoms, it has a different momentum distribution within the target compared to that of the s electrons in helium. The momentum distribution of the ejected electron is known to play a role in the ionization dynamics at high incident energies [10], and so is also expected to play a significant role at the energies studied here.

For krypton and xenon the outer orbital also includes ten electrons in d orbitals. Calculations of the radial probability distribution functions for the outer electrons [11] show there is a significant overlap between the $(n-1)\,d$ electrons and ns and np electrons in each target. The d electrons may therefore also play a role in the ionization dynamics, due to correlations between the bound electrons, and due to polarization of the target during the interaction.

A. Ionization of helium ($V_I = 24.6$ eV)

Figure 2 presents coplanar symmetric data from ionization of helium taken by the spectrometer in Manchester [12]. The data were obtained for excess energies ranging from 3 to 80 eV above V_I. The data are presented as logarithmic

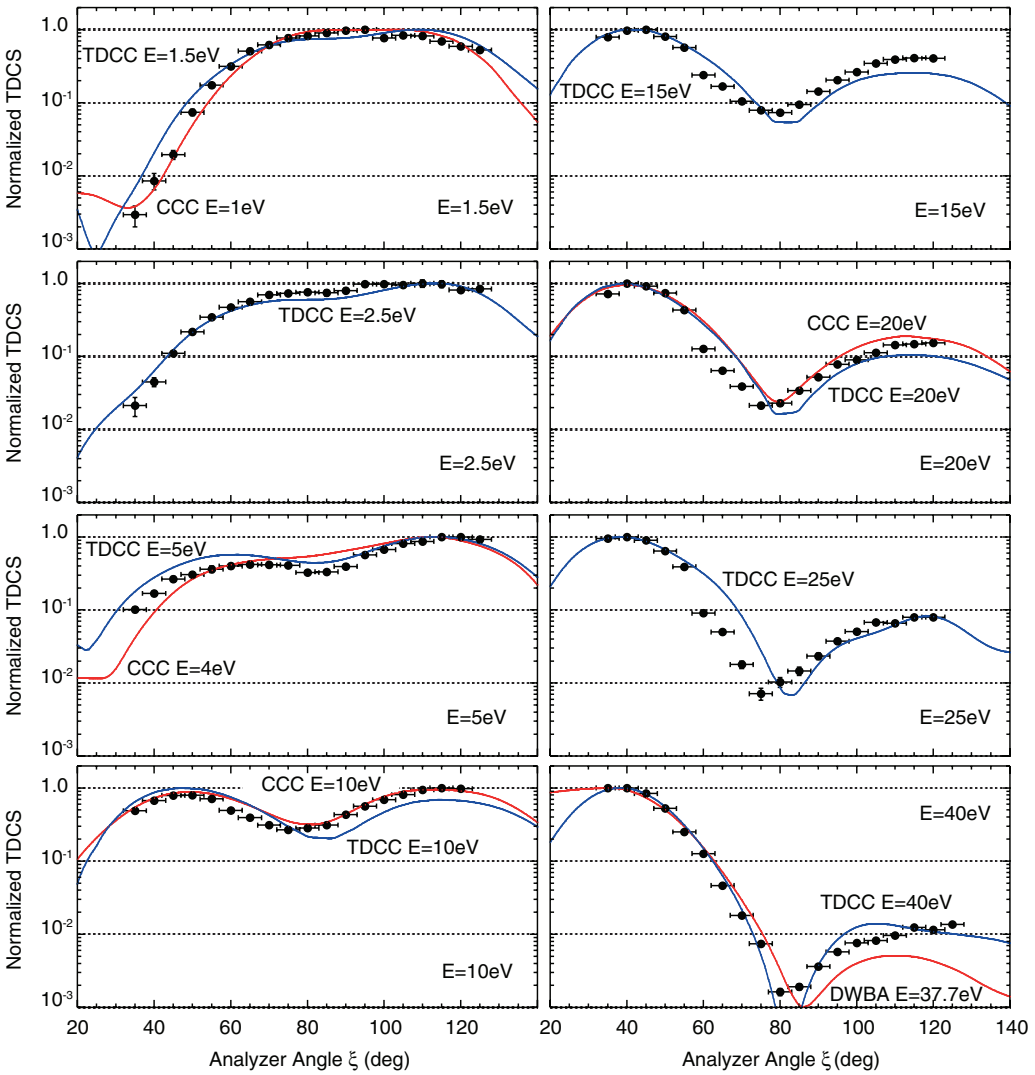

FIG. 2. (Color online) Ionization differential cross sections for helium normalized to unity at the peak of the cross section for each energy. The incident energy ranged from 3 to 80 eV above V_I. The data are compared to published CCC [16] and DWBA calculations [19], as well as recent unpublished TDCC calculations from the Los Alamos National Laboratory group [22].

plots. Note that the DCS at $\xi = 0^\circ$ and $\xi = 180^\circ$ must be zero due to postcollisional interactions between the two outgoing electrons.

At the lowest energy ($E_{\rm inc} = 27.6$ eV; $E = 1.5$ eV) the DCS is a broad featureless peak with a maximum at $\xi = 90^\circ$. At this energy (which is close to threshold) the DCS is considered to be dominated by PCI, as first described by Wannier [13]. In this process electrons emerging from the interaction region with equal low energy are driven away from each other due to their mutual repulsion. As the energy of the electrons reduces to zero, they have correspondingly more time to interact, and so the highest probability of emergence in a coplanar symmetric geometry is when $\xi_1 = \xi_2 = \xi \sim 90^\circ$ (i.e., opposite each other, as observed).

As the electron energy increases out of the threshold region, the dominance of postcollisional interactions decreases, and other scattering mechanisms emerge. Two processes are thought to be most important. The first is a quasifree *binary* collision between incident and bound electrons, resulting in a peak around $\xi = 45^\circ$ (this angle is due to the electrons having equal mass, so that their mutual angle $\xi_1 + \xi_2 \approx 90^\circ$). In this case the ion core that remains after ionization largely acts as a spectator in the collision, and simply balances energy and momentum so that both are conserved. The second important process is considered to be that of a double *recoil* collision. In this case the incident electron initially scatters elastically from the target so as to emerge in the backward direction (i.e., $\mathbf{k_0} \xrightarrow{elastic} -\mathbf{k_0}$), followed by a quasifree collision with a bound electron. The correlated electrons will again emerge at equal angles (as set by the coplanar symmetric geometry chosen here), with a maximum probability at $\xi \sim 135^\circ$. Other processes will also lead to a finite coincidence yield in this geometry; however, binary and recoil collisions are thought to be the most important.

The probability that an elastic collision will deflect the incident electron through 180° (as required for the recoil case) decreases as the incident electron energy increases, as

first calculated by Rutherford. This *backscattering* process is hence expected to be most important at low energies, and should decrease as the energy is raised. By contrast, the single *binary* collision mechanism will increase in importance as the energy increases, and so should dominate the DCS at high energies.

The helium data in Fig. 2 largely confirm the proposed mechanisms. At the lower energies up to around $E = 10$ eV, the DCS is larger in the backward direction than in the forward direction. As the energy increases further, the strength of the forward peak increases relative to the backscatter peak. At $E = 40$ eV the forward peak is ∼100 times stronger than in the backward direction. The maxima in the forward and backward peaks are seen to move from higher ξ angles near threshold towards $\xi = 45^\circ$ and $\xi = 135^\circ$ at the highest energy (although the backscatter peak is beyond the highest angle that can be measured using this instrument). This is in accordance with the important role PCI plays in the measured cross section, as discussed above. A deep minimum also emerges between forward and backward scattering regions as the energy increases. This minimum is nearly 1000 times smaller than the cross section maximum at $E = 40$ eV.

Several state of the art models now closely predict the experimental data for helium. Theories include distorted wave Born approximations (DWBA) [14,15], convergent close coupling theories (CCC) [16], R-matrix formalisms [17], and time-dependent close coupling (TDCC) theories [18]. Of particular note is that each theory uses quite different methods to solve the scattering problem, yet all closely predict the data.

In Fig. 2 the helium data are compared to results from several published models that are close to or at the energies used in the experiment. The CCC calculations of Bray and colleagues [16] are shown at four different energies (E=1, 4, 10, and 20 eV), and an early DWBA calculation by Zhang and co-workers is presented for an incident energy of 100 eV ($E = 37.7$ eV) [19]. The data are also compared to a set of unpublished TDCC results, recently calculated at the specific energies used here [22].

The CCC and TDCC models closely match each other, apart from some small differences in the positions of maxima and minima. At the lower energies the models closely follow the data. The TDCC prediction at $E = 25$ eV is least accurate in emulating the position of the minimum, but closely predicts the relative magnitude of the backscatter peak and the peak positions. The TDCC model slightly overestimates the depth of the minimum at $E = 40$ eV but accurately reproduces the angular position, whereas the DWBA model predicts a small angular shift of the minimum, and slightly underestimates the backscatter peak. All calculations produce results that are in excellent agreement with the experimental data.

The success of these different theoretical approaches has led to the claim that the scattering problem is now effectively "solved" for a helium target [16]. Certainly the close agreement found between theory and experiment shown in Fig. 2 implies that the essential mechanisms controlling the ionization process are being included. As the mass of the noble gas target increases, additional complexity is expected in the interaction, since the number of electrons markedly increases, the size and charge of the nucleus increases, the polarizability of the atom gets larger, and the electrons occupy different orbitals with different angular momenta. Some of the approximations successfully adopted in the models for helium may therefore no longer serve. Disagreements between theory and experiment have been noted for scattering into the perpendicular plane for heavier targets (where comparisons are available), and it remains to be seen if the models can accurately predict the data in the simpler coplanar geometry adopted here.

B. Ionization of neon ($V_I = 21.6$ eV).

A comprehensive set of data for the ionization of neon in a coplanar symmetric geometry are presented in Fig. 3. In this case the incident energy ranged from 1.2 to 200 eV above V_I, so that the evolution of the DCS could be mapped from very close to threshold, through to high energy.

The data are clearly different to that from helium, particularly at lower energies. This indicates that the "simple" descriptions of the scattering mechanisms discussed above for the lighter target are no longer applicable, and more complex interactions are occurring. In particular, the dominance of PCI near threshold is far less obvious, the data at the lowest energies showing a defined peak around $\xi = 65^\circ$, in contrast to the broad featureless structure in helium which peaked at $\xi \sim 90^\circ$. The near-threshold peak in neon clearly evolves into the forward-scattered peak as the energy increases. In contrast to expectations from the recoil model, and in contrast to the data from all other stable noble gas targets, the cross section in the backscatter region from neon is always smaller than in the forward direction. This indicates that at these energies the incident electron has a low probability of penetrating deeply into the core of the target, so as to elastically scatter through 180°.

As the electron energy increases further, a central peak evolves which is most clearly visible at $\xi \sim 85^\circ$ when $E =$ 20 eV. This peak is absent in helium, but has been seen in previous experimental work on this target at intermediate energies [20]. A similar structure is observed in some of the heavier targets. The central peak at $\xi \sim 85^\circ$ is not predicted by the simple binary and backscattering models used to describe ionization from helium; however, the models of Purohit *et al.* [3], Zhang *et al.* [19], and Rioual *et al.* [20] all show that a central feature emanates from a full DWBA calculation. The results from these calculations are reproduced in Fig. 3 where available, at energies close to that used in the present study. Rioual *et al.* [20] suggest this feature may arise from an initial elastic scattering of the electron through 90°, followed by a direct collision combined with deformation of the target orbitals due to polarization. However, since elastic scattering through 90° followed by a binary collision cannot produce a coincidence yield in a coplanar symmetric geometry, it is not clear how this mechanism can reproduce the peak in the DCS, without further collisions that scatter the electrons into opposite directions. The physical mechanism that produces this structure has hence yet to be fully explained.

A clear backscatter peak starts to emerge around $E = 10$ eV which remains distinct at all higher energies. The angle of the maximum in this backscattering peak is not able to be determined due to the limitations of the spectrometer, but in all cases is above $\xi = 130^\circ$. Interestingly the relative strength of the backscatter peak compared to the forward peak *increases* as the energy increases from $E = 10$ eV to

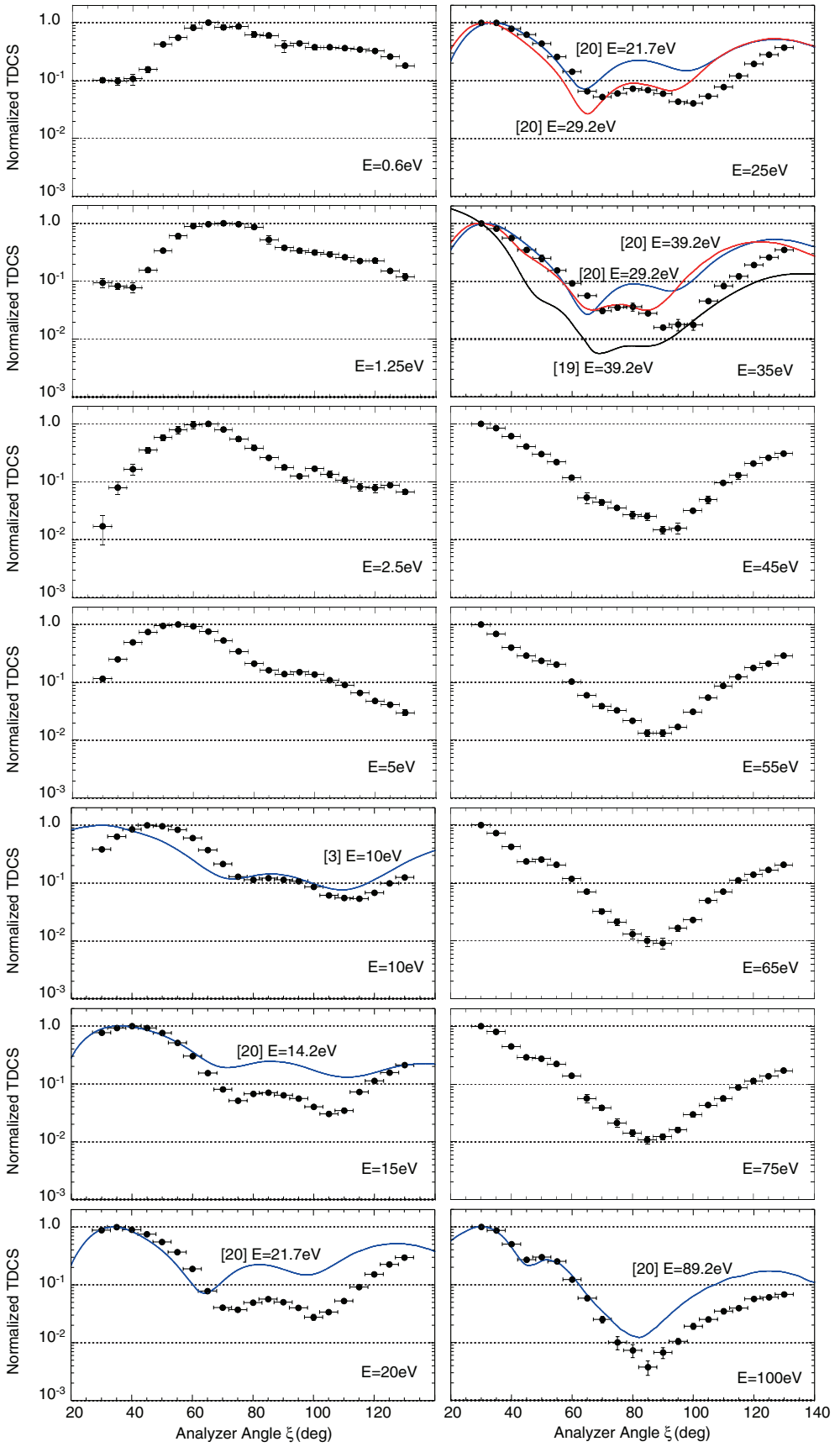

FIG. 3. (Color online) Ionization differential cross sections for neon normalized to unity at the peak of the cross section at each energy. The incident energy ranged from 1.2 to 200 eV above V_I. Examples of previously published DWBA theoretical results at or near the energies used here are also shown [3,19,20], normalized to unity at their peak.

$E = 25$ eV, after which it slowly decreases. This is in contrast to the observations from all other noble gas targets, and is in variance with the recoil model described in Sec. III A.

As the energy increases further, a new dip in the cross section emerges around $\xi = 45^\circ$, which is most clearly visible at the highest energy 200 eV above V_I. This dip occurs since the ionized electron is a p electron, with a bound momentum distribution that is zero when the electron momentum is zero. This type of feature is clearly visible at much higher energies in the coplanar symmetric geometry, since scattering is then dominated by binary collisions [10]. The DWBA calculation for $E = 89.2$ eV clearly shows this feature.

As the energy increases above $E = 35$ eV the central peak around $\xi = 90^\circ$ decreases in magnitude, and is no longer visible at the highest energies. The minimum in the DCS between the central peak and backscatter peak at $\xi \sim 100^\circ$ is seen to evolve into the deep minimum at $\xi \sim 85^\circ$ found at $E = 100$ eV. This minimum in the cross section is ~250 times smaller than the forward-scatter peak at this energy.

Although the DWBA calculations shown in Fig. 3 reproduce the general features of the data, they do not predict the magnitude or positions of the main features. The calculated cross sections are all normalized at their peaks within the angular range of the data, and so there is some flexibility in matching theory to experiment. However, it is clear that significant differences remain, which must be explained in the future.

It is interesting to observe that the overall structure in the DCS for helium and neon are similar at the highest energies, apart from the dip at $\xi = 45^\circ$ due to the different characters of the bound electron before ionization (an s electron for helium, a p electron for neon). This indicates that at higher energies, the scattering process can reasonably be predicted by the binary and recoil mechanisms described in Sec. III A, irrespective of the target. However, as the energy decreases into the intermediate and threshold regions, more complex processes play increasingly important roles. Since the probability of ionization is highest in this energy regime (typically reaching a peak at 5–7 times V_I [21]), it is important that models fully incorporate these mechanisms, so as to accurately predict ionization in this region.

C. Ionization of argon ($V_I = 15.7$ eV)

Figure 4 shows the data obtained for argon. Once again the spectrometer cannot resolve the fine structure splitting of the resulting ion, so the results are an incoherent sum over the cross sections for both ionic ground states. The incident energy ranged from 3 to 100 eV above V_I for this target.

The results differ significantly when compared to helium and neon. Unlike neon, the data at all energies from 3 to 20 eV above V_I show strong backscattering, with a maximum in the cross section occurring for $\xi > 130^\circ$. The backscatter peak remains distinct at all energies to $E = 50$ eV. Surprisingly, and in contrast to the recoil model, the position of the backscatter peak moves to *smaller* angles as the energy increases. This is most easily seen at energies from $E = 30$ eV where the peak position is around $\xi = 125^\circ$ through to $E = 50$ eV where the backscatter peak is a maximum around $\xi = 105^\circ$. This shift in position cannot be due to PCI, and so a different mechanism must be operating.

At low energies a distinct triple-peak structure is seen in the DCS that is most visible at $E = 2.5$ eV. This structure largely disappears at energies above $E = 5$ eV, where the DCS presents a broad flat region between $\xi \sim 55^\circ$ and $\xi \sim 100^\circ$. The relative strength of the forward peak steadily increases until at $E = 15$ eV it is larger than the measured DCS in the backscatter region at the highest angle. As the energy increases further a dip is seen in the forward cross section around $\xi = 45^\circ$ which again is probably due to the ionized electron being a p electron. This dip is most clearly observed at $E = 25$ eV. The dip moves to higher angles as the energy increases, until at $E = 50$ eV it is seen at $\xi \sim 55^\circ$.

It is interesting to note that the minimum in the DCS between the forward and backscatter regions for this target steadily moves from higher angles to lower angles as the energy increases, until at $E = 50$ eV the minimum is at $\xi \sim 80^\circ$. The minimum is deepest relative to the peak in the cross section at an energy $E = 30$ eV; however, at this energy it is only ~80 times smaller than the forward peak. The minimum then becomes shallower as the energy increases further.

At the highest energy where the incident electron energy was 100 eV above V_I, the DCS once again shows the broad features predicted by the binary and recoil models. This indicates these processes once more dominate at high energy. The large variations seen in the DCS as the energy lowers towards threshold show more complex interactions are occurring, which again must be included in the models.

Available theoretical calculations for argon in this energy regime are also depicted in Fig. 4, at energies at or near the energies used in this study. The models predict the position of the minima reasonably well in the backscattering region, although once again the relative magnitudes of different features are not well reproduced. A significant dip in the cross section predicted in the forward direction at around $\xi = 50^\circ$ is not observed.

D. Ionization of krypton ($V_I = 14.1$ eV)

Figure 5 shows the DCS data from krypton. Once again the ion states are not resolved. The incident energy ranged from 3 to 70 eV above V_I for this target, allowing the essential features and structural changes in the DCS to be observed. The data are once again normalized at the peak of the DCS for each energy.

The results at the lowest energies are very similar to those obtained from argon, indicating that the scattering mechanisms that produce the data in this regime are probably similar. At the lowest energy the DCS is relatively featureless and increases in magnitude as the scattering angle increases. At energies of $E = 2.5$ eV and $E = 3.75$ eV a three-peak structure is again seen, which evolves into a broad flat cross section at $E = 5$ eV. A broad forward peak then evolves with a minimum at around $\xi = 100^\circ$. This peak becomes dominant in the measurements around $E = 10$ eV, and remains the largest feature as the energy increases. The position of the forward peak moves from $\xi \sim 60^\circ$ at $E = 7.5$ eV to $\xi \sim 50^\circ$ at $E = 35$ eV. No dip in the forward peak is found, as is observed in neon, argon, and xenon. This is somewhat surprising as the ejected electron in krypton is also a p electron.

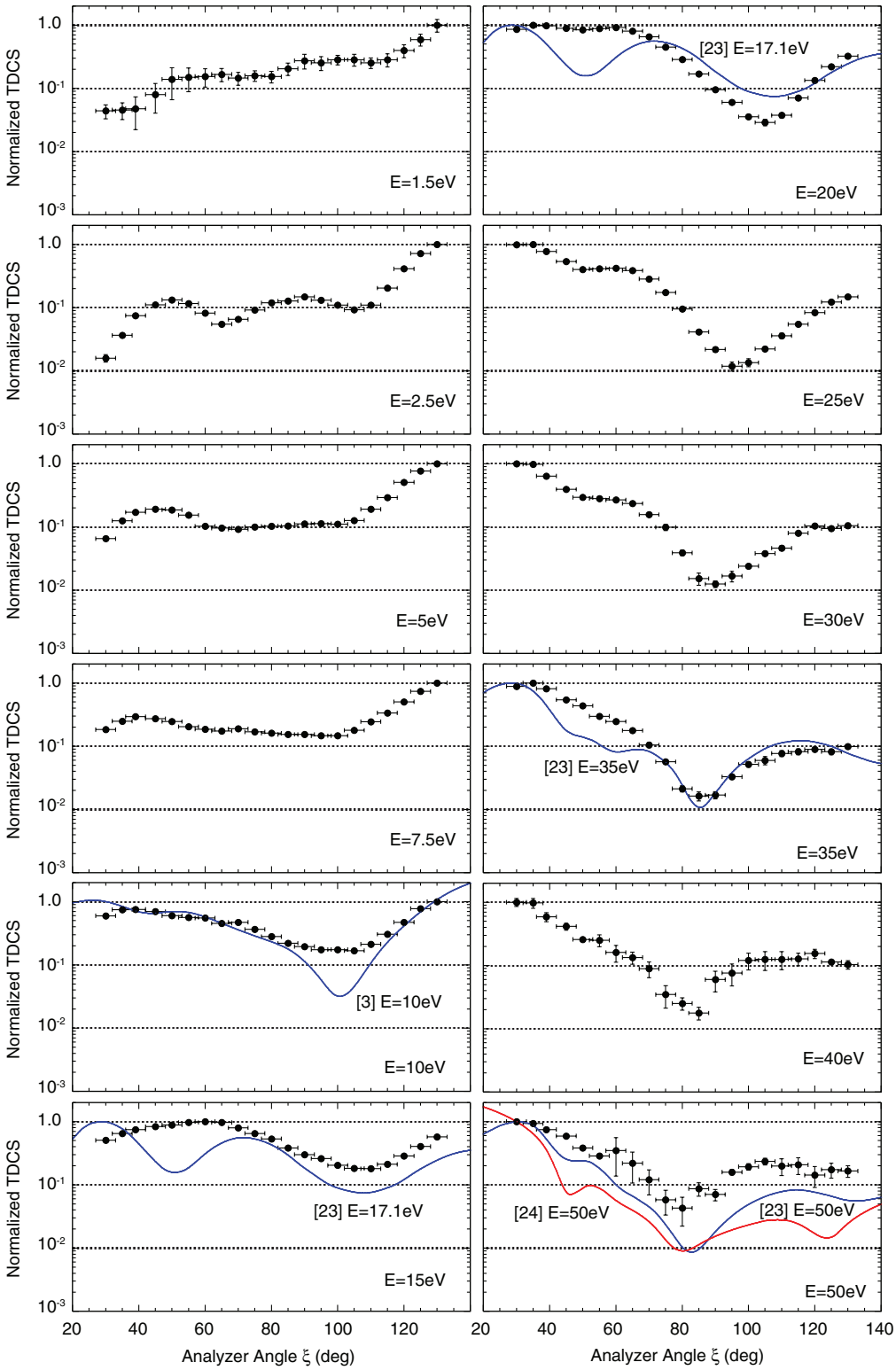

FIG. 4. (Color online) Ionization differential cross sections for argon normalized to unity at the peak of the cross section at each energy. The incident energy ranged from 3 to 100 eV above V_I. Examples of previously published DWBA theoretical results at or near the energies used here are also given [3,23,24], normalized to unity at their peak.

The evolution of the backscatter peak as the energy increases is different for this target. The DCS in the backward direction dominates at energies up to $E = 7.5$ eV, and then steadily decreases in relative magnitude as the energy increases further. At all energies the peak in the backscatter region occurs at an angle above that which can be accessed by the spectrometer. The minimum in the DCS between forward and backscatter regions appears to move to higher angles as the

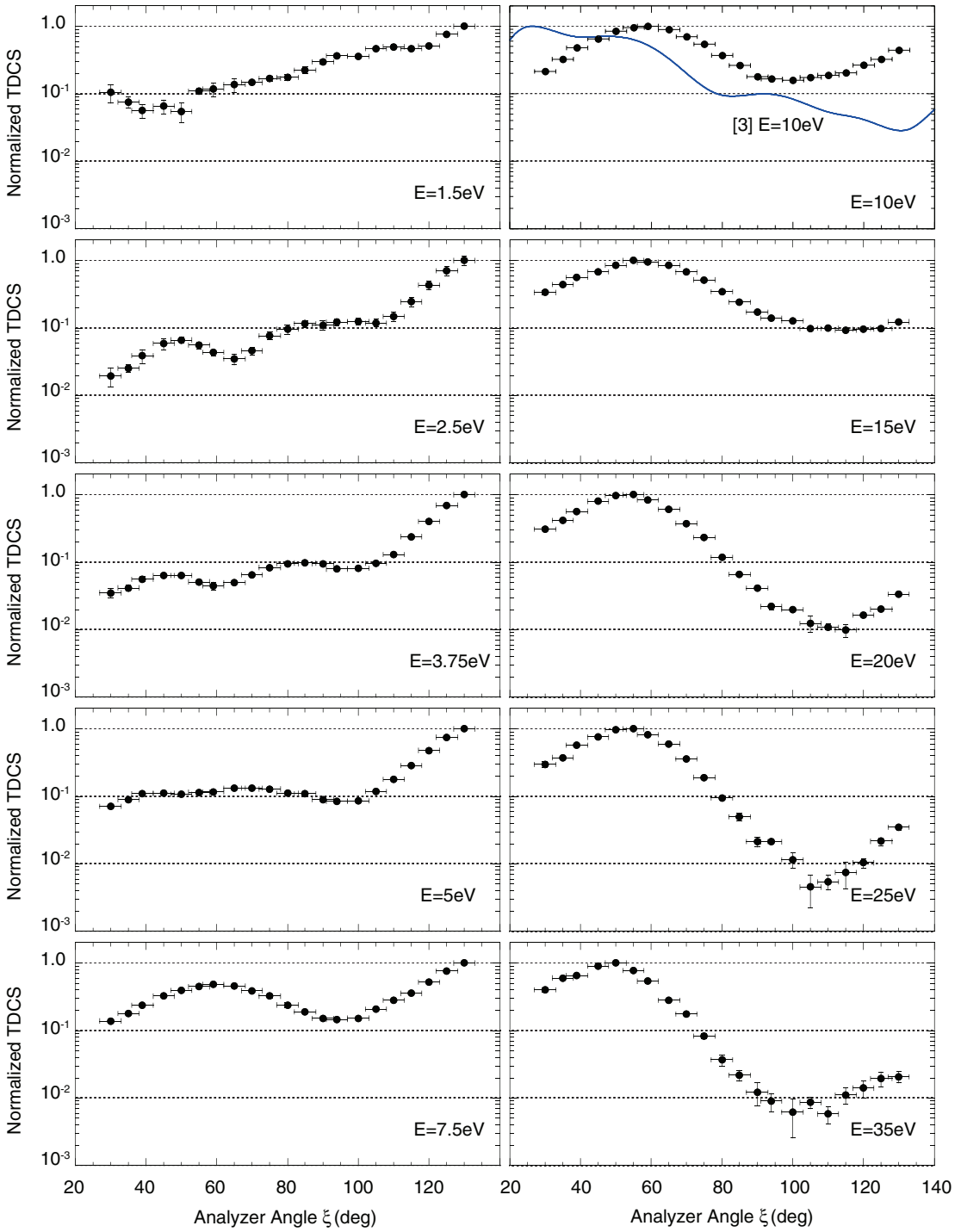

FIG. 5. (Color online) Ionization differential cross sections for krypton normalized to unity at the peak of the cross section at each energy. The incident energy ranged from 3 to 70 eV above V_I. Examples of previously published DWBA theoretical results at $E = 10$ eV are also shown [3], normalized to unity at the peak.

energy increases up to $E = 20$ eV where the minimum is seen at $\xi \sim 115^\circ$, after which the minimum decreases in angle to reach $\xi \sim 100^\circ$ when $E = 35$ eV. This minimum is deepest when $E = 25$ eV where it is ~250 times smaller than the forward peak.

Only one calculation has been found for krypton in this energy regime, using a coplanar symmetric geometry [3]. This is shown for $E = 10$ eV, again normalized to unity at the peak of the cross section. There appears to be little agreement between this calculation and the experimental data.

E. Ionization of xenon to the $^2P_{3/2}$ Xe ion state ($V_I = 12.1$ eV)

Unlike all other targets adopted in this study, it was possible to resolve the fine structure splitting in xenon using the spectrometer in Manchester. Data were hence obtained

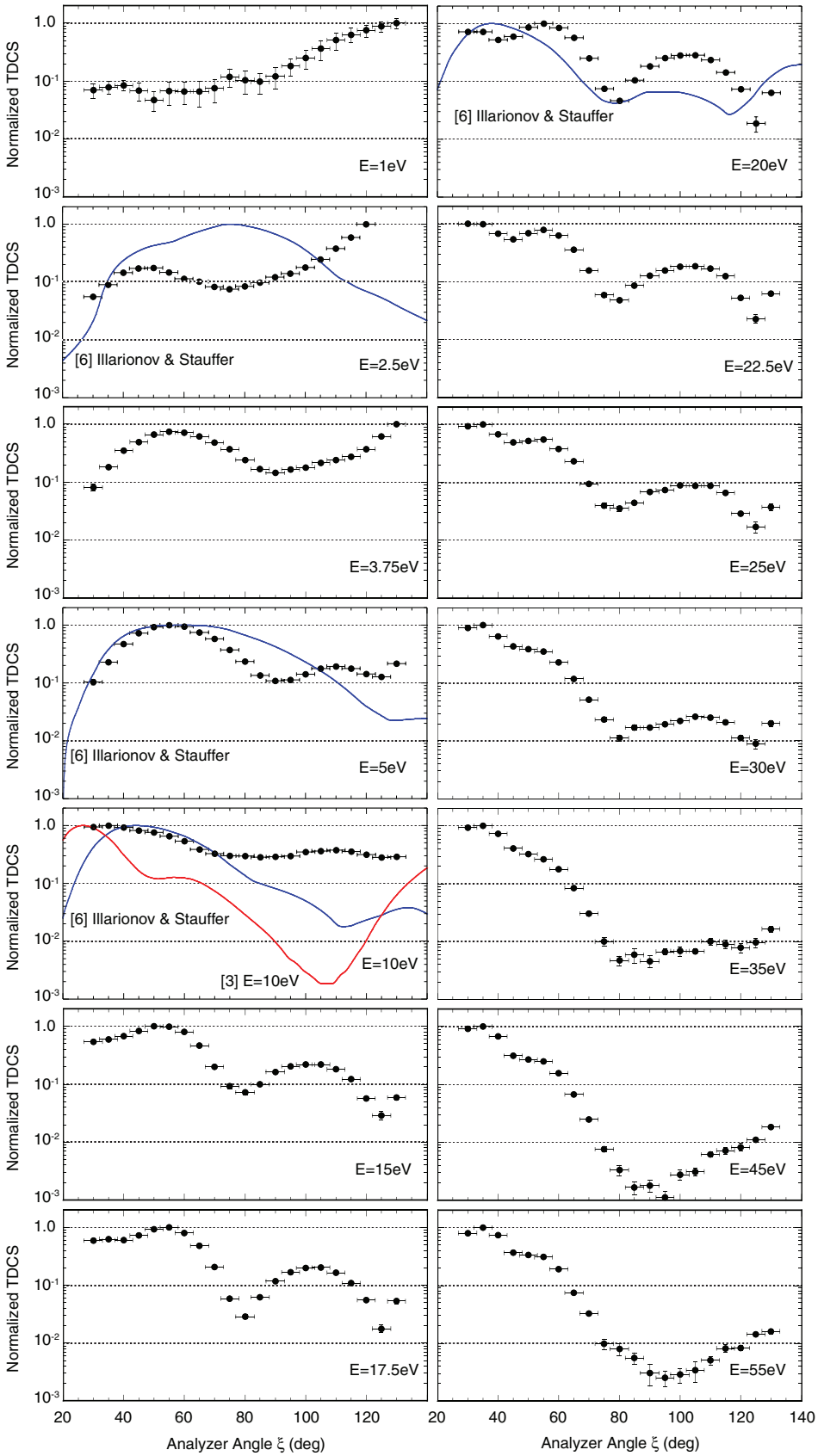

FIG. 6. (Color online) Ionization cross sections to the $^2P_{3/2}$ Xe^+ ion state, normalized to unity at the peak of the cross section at each energy. The incident energy ranged from 3 to 110 eV above V_I. Examples of previously published theoretical results are also shown, normalized to unity at their peak. These include the results from the fully relativistic calculation of Illarionov and Stauffer [6], and results from a nonrelativistic DWBA calculation by Purohit *et al.* [3].

for ionization to the $^2P_{3/2}$ ion state, since this produced the highest yield. The data were obtained from 3 to 110 eV above V_I, as shown in Fig. 6.

At the lowest energy the data for xenon are again similar to those obtained from argon and krypton, with the DCS increasing steadily towards the backscatter region. However,

unlike these lighter targets, a forward peak rapidly emerges as the energy is raised, and is the dominant feature at $E = 5$ eV. The DCS is very different at $E = 10$ eV where it is almost flat, and then changes rapidly once again at $E = 15$ eV and higher energies. Large variations in the scattering process are clearly occurring over this small energy range.

At $E = 15$ eV a three-peak structure is clearly resolved, which becomes four peaks at $E = 20 - 30$ eV. The forward dip around $\xi = 40^\circ$ is again probably due to the ionized electron being a p electron, and it may be that the dip around $\xi = 125^\circ$ is also due to this mechanism (a dip in the DCS due to the p electron momentum distribution would be expected in both forward and backward directions from the binary and recoil models). As the energy increases beyond $E = 30$ eV the peak around $\xi = 105^\circ$ rapidly diminishes, until at $E = 55$ eV the DCS once again shows a similar structure to that in all other targets, with a forward "binary" peak and a backward "recoil" peak. The dip at $\xi \sim 50^\circ$ at $E = 55$ eV is once again probably due to the bound momentum distribution of the ionized p electron. The minimum in the cross section between forward and backward peaks is deepest at $E = 45$ eV, where it is ~1000 times smaller than the forward peak. The relative magnitude of this minimum then increases at $E = 55$ eV, where it is still ~400 times smaller than the forward peak.

Two calculations are available which can be compared to the present data in this energy regime. Purohit and co-workers [3] have calculated the DCS for $E = 10$ eV using a DWBA model that includes polarization and PCI, and Illarionov and Stauffer [6] used a fully relativistic calculation to obtain data over a range of energies. Both calculations have been normalized to unity at their peak for comparison to the data.

The results of the calculations bear little resemblance to the data at all energies where they are available. At the lower energies the calculations predict a peak where the data show a minimum, and a minimum where the data show a peak. The results at $E = 10$ eV in the backscatter region are nearly 100 times larger than calculated. Only at $E = 20$ eV does the relativistic calculation approximate the data, at least in overall magnitude. Clearly both models need to include further scattering mechanisms to more closely describe the experimental results.

IV. CONCLUSIONS

A comprehensive set of ionization coincidence data has been presented that covers a wide range of energies from threshold to relatively high energies, for all of the stable noble gas targets. This is an important region to study these interactions, since the largest probability for direct ionization occurs for incident energies from ~5 to 7 times the ionization potential of the target. A coplanar symmetric geometry was chosen as it allows direct comparison with previous results in the perpendicular plane [2], through the common normalization point when $\xi = 90^\circ$. Since the incident, scattered, and ejected electron momenta all remain in a plane under these conditions, this simplifies the scattering dynamics compared to out-of-plane measurements, and so reduces the complexity of the interaction.

The data from each target presented in Figs. 2–6 show both differences and similarities, depending upon the chosen energy regime. At the highest energy the cross sections for all atoms approach that described by the simpler binary and recoil mechanisms. As the energy is lowered, PCI has to be included together with these scattering mechanisms, and this successfully describes the ionization data obtained from helium. For all other targets, additional complexities arise that are reflected in the changing structures in the observed cross sections. These complexities must be considered in any future models.

Although the results presented here cover a wide range of energies and angles, they do not present the data on an absolute scale. This is due to the practical difficulty of working with low-energy electrons for long periods of time. Since there is a need for *absolute* data at different energies, we intend to address this in the future, by making direct comparison to data obtained from helium. As noted above, the different calculations for the ionization of helium have largely converged over the last 20 years, and are now considered to yield precise predictions of the scattering dynamics and cross sections. By using the results from theory to calculate the efficiencies of the electron optics in the analyzers and electron gun, it should then be possible to place the results presented here on an absolute scale. The results of such a study will be presented in a future paper.

ACKNOWLEDGMENTS

The work presented here could not be carried out without the continued technical expertise of the mechanical workshop in the Schuster laboratory, who help to maintain the (e,2e) spectrometer in Manchester. K.L.N. would also like to thank the European commission for providing a Marie Curie incoming Fellowship during this time. The authors would also like to thank Dr. James Colgan and Dr. Gregory Armstrong and the Los Alamos National Laboratory for providing their unpublished TDCC calculations for the ionization of helium at the energies used in this study.

[1] K. L. Nixon, A. J. Murray, and C. Kaiser, J. Phys. B **43**, 085202 (2010).
[2] K. L. Nixon and A. J. Murray, Phys. Rev. A **85**, 022716 (2012).
[3] G. Purohit, A. S. Bhullar, and K. K. Sud, Ind. J. Phys., B **77**, 177 (2003).
[4] G. Purohit, P. Singh, V. Patidar, Y. Azuma, and K. K. Sud, Phys. Rev. A **85**, 022714 (2012).
[5] A. Williart and G. Garcia, Phys. Scr. **64**, 343 (2001).
[6] A. A. Illarionov and A. D. Stauffer, J. Phys. B **45**, 225202 (2012).
[7] A. J. Murray, in *Fragmentation Processes*, edited by C. T. Whelan (Cambridge University Press, Cambridge, 2013), p. 164.
[8] A. J. Murray, B. C. H. Turton, and F. H. Read, Rev. Sci. Instrum. **63**, 3346 (1992).
[9] J. N. H. Brunt, G. C. King, and F. H. Read, J. Phys. B **10**, 1289 (1977).

[10] G. Stefani, R. Camilloni, and A. Giardini-Guidonu, J. Phys. B **12**, 2583 (1979).
[11] E. Clementi and C. Roetti, At. Data Nucl. Data Tables **14**, 177 (1974).
[12] A. J. Murray and F. H. Read, Phys. Rev. A **47**, 3724 (1993).
[13] G. H. Wannier, Phys. Rev. **90**, 817 (1953).
[14] J. M. Martinez, H. R. J. Walters, and C. T. Whelan, J. Phys. B **41**, 065202 (2008).
[15] O. Al-Hagan, C. Kaiser, D. H. Madison, and A. J. Murray, Nat. Phys. **5**, 59 (2009).
[16] I. Bray, D. V. Fursa, A. S. Kadyrov, and A. T. Stelbovics, Phys. Rev. A **81**, 062704 (2010).
[17] O. Zatsarinny and K. Bartschat, Phys. Rev. A **85**, 062709 (2012).
[18] J. Colgan, O. Al-Hagan, D. H. Madison, A. J. Murray, and M. S. Pindzola, J. Phys. B **42**, 171001 (2009).
[19] X. Zhang, C. T. Whelan, and H. R. J. Walters, J. Phys. B **23**, L509 (1990).
[20] S. Rioual, A. Pochat, F. Gelebart, R. J. Allan, C. T. Whelan, and H. R. J. Walters, J. Phys. B **28**, 5317 (1995).
[21] P. L. Bartlett and A. T. Stelbovics, Phys. Rev. A **66**, 012707 (2002).
[22] G. S. J. Armstrong and J. Colgan (private communication, 2013).
[23] S. Rioual, B. Rouvellou, A. Pochat, J. Rasch, H. R. J. Walters, C. T. Whelan, and R. J. Allan, J. Phys. B **30**, L475 (1997).
[24] S. Bell, C. T. Gibson, and B. Lohmann, Phys. Rev. A **51**, 2623 (1995).